Nanoscale

PAPER

View Article Online
View Journal | View Issue

Cite this: *Nanoscale*, 2025, **17**, 25254

Study of the biomolecular corona of surface-modified polystyrene and silica nanoparticles: application to cancer

Antonietta Greco, †[a] Esther Imperlini, †[b] Gha Young Lee,[c] Maciej Serda,[d] Santiago Alonso Tobar Leitão[e] and Claudia Corbo *[a,f]

Received 21st July 2025,
Accepted 21st October 2025

DOI: 10.1039/d5nr03082j

rsc.li/nanoscale

Nanotechnology offers promising tools for disease diagnosis through the unique biomolecular corona (BC) that surrounds nanoparticles (NPs) when exposed to biological fluids, creating personalized profiles. In this study, we investigated the capability of BC of polystyrene and silica NPs with diverse surface functionalization in distinguishing eight types of cancer (breast, ovarian, kidney, lung, colon, bladder, uterus, and thyroid) using a straightforward method based on one-dimensional gel electrophoresis. A total of six NPs, silica and polystyrene NPs with various functional groups (plain, NH_2, and COOH), were exposed to a total of 43 plasmas, 5 for each of the 8 investigated cancers plus 3 controls, to create personalized BCs. By analyzing the densitometric profiles of proteins' molecular weights, we demonstrated that the BC signatures of NPs can distinguish healthy individuals from those affected by cancer. We revealed that certain BCs could discriminate against specific types of cancer, *i.e.* ovarian and kidney cancer, and that amination could improve the diagnostic power of the platform. Being fast, cheap, and requiring only a blood sample, if validated on a more comprehensive cohort of patients, this method could serve as a first-line diagnostic tool, guiding decisions on further invasive testing and/or patient monitoring post-surgery or during treatment.

Introduction

The biological fate of nanoparticles (NPs) is governed by their specific interactions with biomolecules that naturally adsorb onto their surface.[1] When NPs enter biological environments, they become coated with a dynamic layer of biomolecules, forming what is known as the biomolecular corona (BC). The resulting BC-NPs complexes then interact with cell membranes and intracellular organelles, influencing cellular uptake, distribution, and biological response.[2,3] The BC has been extensively studied over the past decade, particularly for its impact on the targeting capabilities of nanosized delivery systems.[4] More recently, research has focused on engineering an artificial BC to enhance specific desired features.[2,5,6] For example, the incorporation of quaternary ammonium lipids into lipid NPs (LNPs) allowed modulating the BC composition, abundant in Apolipoproteins (306-O12B LNPs) or in coagulation-relevant proteins (306-N16B LNPs), and selectively reaching lung cells.[7–11]

Giulimondi and colleagues utilized the negative charge of DNA to coat non-PEGylated liposomes forming lipoplexes. Interestingly, upon exposure to human plasma, these lipoplexes developed a BC with a notably low opsonin content (only 5%), a condition essential to reduce the nanocarriers' immune system recognition and prolong their circulation time.[12] Luo and colleagues obtained similar results by stabilizing Cabazitaxel nanocrystals with D-α-Tocopherol PEG 1000 succinate which favoured the preferential interaction with Serum Albumin, Apolipoprotein A-IV, Apolipoprotein E, and Transferrin. As a result, the nanocrystals had a prolonged circulation time and were able to target the tumour in 4T1 orthotopic tumour-bearing mice.[13] An interesting study by Peng and collaborators involved coating pheophytin carbon dots with 1,2-distearoyl-*sn-glycero*-3-phosphoethanolamine (DSPE)-mPEG, resulting in the formation of a BC predominantly composed of Apolipoprotein A-I, Apolipoprotein C-III, and Apolipoprotein E. This specific corona composition facilitated the interaction of the NPs with cancer cells expressing low-density lipoprotein receptors (LDLR).[14]

As well established, BC's composition strongly depends on both the physicochemical properties of NPs (*e.g.*, material

[a]*University of Milano-Bicocca, Department of Medicine and Surgery, NANOMIB Center, Monza 20900, Italy. E-mail: claudia.corbo@unimib.it*
[b]*Department for Innovation in Biological, Agrofood and Forest Systems, University of Tuscia, 01100 Viterbo, Italy*
[c]*Center for Nanomedicine and Department of Anaesthesiology, Brigham and Women's Hospital, Harvard Medical School, Boston, MA, USA*
[d]*Institute of Chemistry, University of Silesia in Katowice, Poland*
[e]*Hospital Moinhos de Vento PROADI-SUS, Porto Alegre/RS, Brazil*
[f]*IRCCS Istituto Ortopedico Galeazzi, Milan 20161, Italy*
†These authors contributed equally.

type, shape, size, surface functionalization) and the characteristics of the biological milieu (*e.g.*, plasma from healthy or diseased individuals).[2,7,15,16] Indeed, beyond the well-known impact of the BC on the targeting, delivery, and circulation time of NPs,[17] a particularly interesting aspect, investigated by our group and others, is the BC's ability to provide molecular fingerprints that reflect disease states, including cancer. Noteworthy studies in this field have explored the exploitation of the BC for the detection of biomarkers and molecular patterns, highlighting its potential for diagnostic applications.[15] Indeed, the BC of a plethora of NPs has been used to develop methods for diagnosis of Alzheimer's disease, sepsis, coronary artery disease, breast cancer, prostate cancer, lung cancer, pancreatic cancer, and melanoma.[18–27] This emerging approach has great potential for minimally invasive cancer diagnosis. However, the high cost of the BC's analysis, which often requires mass spectrometry, represents a challenge.[15] To bypass this step, Caracciolo's group investigated the diagnostic potential of mass spectrometry-free analysis of BCs formed on clinically approved liposomes. They were able to combine physical measurements after BC formation with data from semi-quantitative densitometric analysis of gel electrophoresis bands to differentiate characteristics between the BCs of breast, gastric, and pancreatic cancer.[28] Similarly, using one-dimensional gel electrophoresis to analyse the BC on graphene oxide (GO) and LNPs, the same group demonstrated to successfully discriminate glioblastoma and pancreatic cancer patients from healthy controls, with a classification accuracy in the case of pancreatic cancer of 88%.[29,30] Di Giacomo *et al.* developed a multiplex point-of-care test for pancreatic ductal adenocarcinoma (PDAC) by integrating inflammatory biomarkers, standard laboratory parameters, and protein corona-based blood assays. The test generated a risk score that accurately distinguished PDAC patients from healthy controls (88.9% specificity, 93.6% sensitivity).[31] Moreover, the same group showed that combining CA 19-9 levels with a GO-based corona assay analysed *via* gel electrophoresis further improved pancreatic cancer classification accuracy, reinforcing the potential of this approach for personalized clinical decision-making.[32] Another mass spectrometry-free approach for analysing BCs implies the use of Transmission Electron Microscopy (TEM). For example, Sheibani and colleagues investigated the distribution, morphology, and association of BCs adsorbed onto carboxylated polystyrene NPs using high-resolution TEM, cryo-TEM, and general image analysis, with the aim of uncovering the biological identity of the NPs.[33] Wu *et al.*, investigated the formation and features of BC formed on the surface of iron oxide NPs by dynamic light scattering (DLS), NPs tracking analysis, flow cytometry, and TEM.[34] Interestingly, Dell'Aglio and colleagues demonstrated that the use of Laser-Induced Breakdown Spectroscopy (NELIBS) allowed to sense the BC of gold NPs by avoiding the mass spectrometry analysis.[35] In contrast to previous studies that relied on single-NP approaches, herein we use a panel of six distinct NPs, each differing in physicochemical properties (*e.g.*, surface charge, and composition). This multi-particle system enables the formation of diverse BC fingerprints when exposed to blood plasma, significantly enhancing the sensitivity and specificity of cancer detection. Notably, we evaluated its potential across multiple cancer types (8 types), thereby highlighting its broader applicability. To this end, we employed six NPs: three types of silica with various functional groups (plain, NH_2, and COOH, named Si, Si-NH_2, and Si-COOH, respectively) and three types of polystyrene with different functional groups (plain, NH_2, and COOH, named Poly, Poly-NH_2, and Poly-COOH, respectively). Each of these NPs was exposed to the plasma of cancer patients (n = 40, clinical information provided in Table S1) affected by one of the following eight types of tumours (breast, ovarian, kidney, lung, colon, bladder, uterus, and thyroid; n = 5 each) and plasma from healthy control individuals (n = 3), to create disease-specific or control BCs. By utilizing this panel of NPs with diverse core materials and surface functionalization, we aimed to capture distinct yet complementary BCs from each plasma sample. We hypothesized that analysing these multiple and varied BC profiles would provide a multi-dimensional dataset, enhancing the ability to generate unique signatures and improve discrimination between different cancer types and healthy states. The resulting BCs were analysed using sodium dodecyl sulfate-polyacrylamide gel electrophoresis (SDS-PAGE). In total, we analysed 258 BCs leading to the generation of a rich, multi-dimensional dataset of protein signatures capable of distinguishing healthy individuals from patients with eight different types of cancer. The experimental workflow is summarized in the schematic (Fig. 1).

Experimental section

Materials

Polystyrene and silica NPs were purchased from Polyscience, Inc. (https://www.polysciences.com/) and Kisker-Products (https://www.kisker-biotech.com/) respectively. Human plasma from cancer patients and healthy individuals was obtained from Innovative Research, Inc. (Novi, MI, USA). Bradford, Laemmli buffer 2X, and 4–20% Mini-PROTEAN® TGX™ Precast Gels were supplied by Bio-Rad Laboratories, Hercules, CA. Coomassie Brilliant Blue was obtained from Fisher Scientific, Fair Lawn, NJ, USA.

Nanoparticles

In this study, we employed six types of NPs with a nominal diameter of approximately 100 nm, composed of polystyrene or silica and functionalized with either plain (Poly and Si, respectively), amino-conjugated (Poly-NH_2 and Si-NH_2), or carboxyl-conjugated surfaces (Poly-COOH and Si-COOH). Silica NPs were supplied by Kisker-Products (https://www.kisker-biotech.com/), while polystyrene NPs were purchased from Polyscience, Inc. (https://www.polysciences.com/). Both manufacturers follow standardized synthesis protocols and quality control procedures to ensure high batch-to-batch reproducibility. Each batch was characterized by the suppliers using tech-

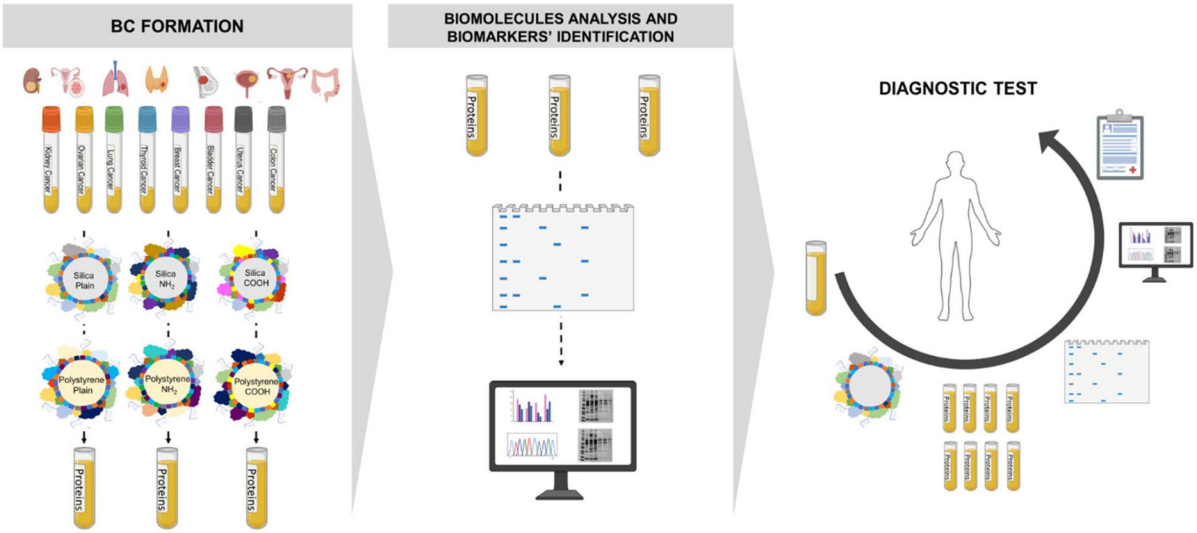

Fig. 1 Schematic representation of the BC analysis workflow. Polystyrene and silica NPs were incubated with plasma derived from patients (kidney, ovarian, lung, thyroid, breast, uterus, and colon cancer) and healthy donors. The obtained BCs were isolated and analyzed using SDS-PAGE. Significant differences were found between healthy and cancer-affected donors by evaluating lane band intensity by densitometric analysis. This workflow represents a proof-of-concept for the early diagnosis of disease and holds potential for guiding treatment decisions. Created in https://BioRender.com.

niques such as DLS and zeta potential (*Z*-pot) measurements to confirm homogeneity in size distribution, surface charge, and functionalization.

Physicochemical characterization of nanoparticles

The size and surface charge (*Z*-pot) of both NPs and BC-coated NPs were characterized using NPs tracking analysis (Nanosight, Malvern, UK) and Zetasizer Nano ZS90 (Malvern, UK), respectively. Briefly, NPs were diluted in water to reach a concentration of 50 μg mL^{-1}. Size and surface charge values are reported as mean ± standard error (SE) of three independent measurements. For TEM morphological analysis, samples and grids were labelled with 1% uranyl acetate. Samples were adsorbed to the grid by floating the grid on a drop of sample for 1 min, liquid excess was removed with filter paper (Whatman #1). A Tecnai G2 Spirit BioTWIN TEM equipped with an Hamamatus ORCA HR camera (80 kV), with a magnification of 68k×, was used.

Cancer biomolecular corona formation

Human plasma from cancer patients and healthy individuals was purchased from Innovative Research, Inc. (Novi, MI, USA). Blood samples collected in K_2EDTA tubes were centrifuged at 500*g* for 20 minutes at room temperature. The plasma supernatant was carefully transferred to a new conical tube without disturbing the cell layer. To further purify the plasma, a second centrifugation was performed at 1000*g* for 5–10 minutes at room temperature. Plasma was aliquoted and freezed at ≤−70° C for long-term storage. To create BCs on each of the six NPs types, plasma samples from patients with eight diverse cancer types (n = 5 for each type: breast, ovarian, kidney, lung, colon, bladder, uterus, and thyroid) and healthy individuals (n = 3) were used, resulting in a total of 258 BCs for formation and analysis. The BCs were prepared by incubating 0.5 mg of NPs at 37 °C for 1 h with 200 μL of human plasma samples diluted with 200 μL of deionized H_2O (final plasma concentration 50% v/v). After incubation, BC-NPs complexes were separated by centrifugation at 14 000 rpm at 4 °C for 30 min and washed three times with cold phosphate-buffered saline (PBS, 4 °C) to remove the loosely-bound, 'soft' BC. The resulting BC-coated NPs, now enriched with the 'hard' corona, were resuspended in a denaturing buffer (8 M urea and 50 mM ammonium bicarbonate) for SDS gel electrophoresis. The proteins concentration within the BC was determined by Bradford assay according to the manufacturer's protocol (Bio-Rad Laboratories, Hercules, CA) using albumin for the standard curve.

SDS gel electrophoresis and densitometric analyses

An equal volume of Laemmli buffer 2× (Bio-Rad Laboratories, Hercules, CA) was added to BCs dissolved in 8 M Urea and 50 mM ammonium bicarbonate. After incubation at 90 °C for 5 min, proteins were loaded and resolved on a 4–20% Mini-PROTEAN® TGX™ Pre-cast Gels (Bio-Rad Laboratories, Hercules, CA) for 1 h at 120 V. Protein bands in the gels were stained with Coomassie Brilliant Blue (Fisher Scientific, Fair Lawn, NJ, USA) overnight followed by extensive washing in ultra-pure water. Gel images were acquired using the GelDoc Go Gel Imaging System (Bio-Rad Laboratories, Hercules, CA), and densitometric analysis of the protein bands was then performed. Gel lanes were analysed to obtain an integral density value using ImageJ software (website: imagej.nih.gov/ij/). Specifically, a vertical rectangle spanning the full height of the 4–20% gel was drawn over the first lane, corresponding to the molecular weight ladder. This same rectangle was then moved

across to each subsequent lane within the gel. To ensure accuracy and reproducibility, the width of the rectangle was carefully selected to avoid overlapping with adjacent lanes while encompassing all the bands present in each lane. To account for potential variations between gels, in each gel, the raw densitometry signal of each lane was normalized using the corresponding gel's molecular weight ladder, whose total lane intensity was arbitrarily fixed to one.

Statistical analysis

All results are presented as mean value ± standard deviation (SD) or mean value ± SE as specified. Statistical significance was investigated using one-way ANOVA with Tukey's multiple comparison test and Unpaired *t*-test. All the statistical evaluations including the receiver operating characteristic (ROC) curve and area under the curve (AUC) analyses were performed in GraphPad Prism version 8.3.0. (GraphPad Software Inc., La Jolla, CA, USA).

Results and discussion

Nanoparticle characterization and biomolecular corona formation

The nano-sized platform used for the diagnostic method study consisted of six NPs with different surface modifications, based on expected differences in protein affinity to obtain variable BC profiles upon incubation in plasma samples (healthy and cancer). As widely known, batch-to-batch variability in NPs synthesis could influence their features (*e.g.*, charge, size, and hydrophobicity) thereby impacting protein adsorption and BC formation. To minimize such an effect, in our study we employed NPs provided by reputable manufacturers that adhere to robust standardized protocols of synthesis, ensuring high reproducibility and consistency across different batches. All six NPs, before BC creation, had a diameter of approximately 100 nm and a negatively charged surface, confirming the manufacturer's specifications (Fig. S1a). We decided to restrict the NPs library to negatively charged NPs with the aim of avoiding non-specific interactions while promoting the absorption of low abundant diagnostically informative proteins in the BC. Indeed, at physiological pH, most plasma proteins present a net negative charge and positively charged NPs are prone to strong electrostatic interactions that favour non-specific adsorption of highly abundant proteins such as albumin and immunoglobulins. This phenomenon often leads to dense BC dominated by non-informative proteins, which may hide the enrichment of diagnostically relevant, lower-abundance species. By contrast, negatively charged NPs tend to promote more selective and differential binding profiles, in line with the diagnostic aims of this study.[36–39] Interestingly, after plasma incubation, all NPs exhibited an enlargement in size up to 44 nm, and most of them showed an increase in *Z*-Pot becoming less negative, as reported in Table 1.

Notably, this trend was not observed in the Poly-NH_2 NPs, which consistently exhibited a decrease in the *Z*-Pot value (*i.e.*, becoming more negative) after plasma incubation. For example, bare Poly-NH_2 had an initial *Z*-Pot of −19.33 mV (Fig. S1) which decreased to −37.38 mV after incubation with breast cancer plasma, corresponding to a change of −18.05 mV (Table 1). This behaviour could be related to the specific adsorption of negatively charged proteins *via* electrostatic interaction between the amino groups on the NPs surface and negatively charged proteins in plasma.[18,40,41]

Morphological analysis by TEM revealed that NPs exhibited a homogeneous spherical shape and smooth surface, condition preserved also after the plasma incubation (Fig. S1b and d).

Moreover, TEM images revealed the presence of a distinct, coating surrounding the NPs following incubation with plasma (Fig. S1d). This coating is indicative of the formation of a BC, suggesting adsorption of plasma proteins and other biomolecules onto the NP surface. Indeed, NPs displayed an overall increase in size following plasma incubation, consistent with the results obtained from DLS analysis.

To investigate the correlation between NPs physicochemical properties and BC composition, we performed a statistical analysis of the post-incubation DLS data, including size and *Z*-Pot (Table S2). One-Way ANOVA statistical analysis of post-incubation data relative to size showed that in general polystyrene NPs could discriminate cancer BC *vs.* control better than silica NPs. In particular, Poly-NH_2 showed statistically significant differences with all of the eight cancer types, while Poly and Poly-COOH NPs showed significant differences with seven of the eight cancer types (Table S2a).

The statistical analysis of the post-incubation *Z*-Pot values revealed a positive significant general trend, for both polystyrene and silica NPS, in discriminating cancer BC *vs*. control (Table S2b).

Altogether, these results indicate that, although plasma incubation generally induces measurable alterations in NPs size and charge surface, the magnitude and significance of these effects depend on both NPs chemistry and pathological condition. This variability suggests that the interaction between NPs and the BC corona may display a degree of selectivity, potentially reflecting disease-specific conditions. At this stage, these notable preliminary results could not represent by themselves a discriminating factor in cancer detection, as they are not informative about the proteins in the BC that could have a role in the discrimination.

Thus, to obtain a more comprehensive overview of the BC composition and its potential role in cancer-specific signatures, we performed SDS-PAGE analysis.

SDS-PAGE analysis of biomolecular coronas

In recent years, the study of BC for the early diagnosis of different diseases has increased due to the correlation between BC composition and the alteration of plasma proteins in pathological conditions.[2,3,7,22] Indeed, plasma from different donors is known to vary in protein content and other biochemical features, all of which may influence BC formation.[18] In this study, to mitigate this factor, plasma samples were randomized across subjects within each cancer type and healthy

Table 1 Characterization of NPs incubated health and cancer plasma. Results represent the mean ± SE of 5 independent batches (n = 5). The size increase and Z-pot variation are referred to the comparison with the NPs analyzed in water

	NPs	Size (nm)	SE	Size increase (nm)	Z-Pot (mV)	SE	Z-Pot variation (mV)
Brest cancer	Poly	117.8	2.7	13.10	−13.35	0.39	19
	Poly-NH_2	158.5	5.3	28.95	−37.38	0.69	−18.05
	Poly-COOH	121.7	1.9	12.75	−31.11	0.51	3.06
	Si	177.8	13.9	44.20	−13.65	1.06	16.33
	Si-NH_2	134.1	9	26.70	−19.56	1.05	13.39
	Si-COOH	175.7	37	38.05	−22.47	1.62	4.55
Colon cancer	Poly	110.2	0.7	9.3	−12.48	0.41	19.87
	Poly-NH_2	131	5.3	15.2	−34.22	1.22	−14.89
	Poly-COOH	101.7	1.8	2.75	−28.89	0.64	5.28
	Si	160.4	29.9	35.50	−28.55	0.49	1.43
	Si-NH_2	134.6	2.5	26.95	−32.23	0.53	0.72
	Si-COOH	145.4	4.9	22.90	−32.87	1.31	−5.85
Uterus cancer	Poly	107.9	2	8.15	−11.91	1.8	20.44
	Poly-NH_2	121.5	0.3	10.45	−30.86	0.87	−11.53
	Poly-COOH	109.6	3.8	6.70	−38.64	0.32	−4.47
	Si	102.7	4.7	6.65	−4.28	0.93	25.70
	Si-NH_2	108.7	2.6	14	−24.46	0.34	8.49
	Si-COOH	156.4	19.6	28.4	−30.30	0.95	−3.28
Ovarian cancer	Poly	153.6	16.8	31	−17.34	1.05	15.01
	Poly-NH_2	118.2	1.4	8.8	−25.31	1.24	−5.98
	Poly-COOH	102.5	1.9	3.15	−26.59	0.89	7.58
	Si	109.9	4.4	10.25	−16.02	1.49	13.96
	Si-NH_2	139.8	13.4	29.55	−5.2	0.52	27.75
	Si-COOH	136.2	7.1	18.3	−22.94	1.86	4.08
Kidney cancer	Poly	114.3	5.4	11.35	−27.71	0.55	4.64
	Poly-NH_2	117.8	2.3	8.6	−30.81	0.47	−11.48
	Poly-COOH	103.3	1.1	3.55	−29.56	1.42	4.61
	Si	140.6	12.2	25.6	−18.99	1.1	10.99
	Si-NH_2	152	21.4	35.65	−16.73	0.81	16.22
	Si-COOH	148.1	9.3	24.25	−23.85	0.88	3.17
Lung cancer	Poly	101.9	1.8	5.15	−12.04	1.63	20.31
	Poly-NH_2	126.8	2	13.1	−26.42	0.4	−7.09
	Poly-COOH	116.3	3.2	10.05	−25.99	0.83	8.18
	Si	105.4	16.1	8	−5.42	0.38	24.56
	Si-NH_2	101.5	2.3	10.4	−10.23	0.43	22.72
	Si-COOH	160.9	4.9	30.65	−15.3	0.69	11.72
Thyroid cancer	Poly	111.4	1.3	9.9	−9.36	0.27	22.99
	Poly-NH_2	120.1	3.5	9.75	−33.8	0.13	−14.47
	Poly-COOH	112.1	4.5	7.95	−21.51	0.85	12.66
	Si	122.1	3.6	16.35	−10.12	0.62	19.86
	Si-NH_2	113	3	16.15	−19.55	1.16	13.4
	Si-COOH	115.4	4	7.9	−18.73	0.84	8.29
Bladder cancer	Poly	107.2	5.8	7.8	−9.84	0.38	22.51
	Poly-NH_2	111.2	2.3	5.3	−26.15	1.97	−6.82
	Poly-COOH	167.7	2.4	35.75	−25.49	1.26	8.68
	Si	124.4	5.9	17.5	−9.56	0.51	20.42
	Si-NH_2	136.2	1.6	27.75	−18.54	0.5	14.41
	Si-COOH	143.7	8.6	22.05	−24.15	1.44	2.87

control group. This approach minimizes systematic bias related to individual variability while still allowing us to capture biologically relevant diversity. Despite some degree of unavoidable inter-individual variability, we observed consistent trends in protein adsorption. Specifically, the overall patterns of BC formation, including size, Z-Pot changes, and BC protein profiles, remain robust across individuals within each group, which strengthens the relevance of the observed trends for cancer detection.

The BCs were analysed by SDS-PAGE and subsequently stained with Coomassie Brilliant Blue for protein visualization and further densitometric analysis (Fig. 2 and Fig. S2). Before loading, the protein amounts comprising the various BCs isolated from the six NPs, were quantified using the Bradford assay (Table 2), thus resulting in total protein amounts in the range from 25 to 40 μg.

To confirm that the bands observed were specific to the BC and not related to potential contamination from unbound proteins, we performed an SDS-PAGE also on n = 3 non-oncological plasma samples (without NPs). In addition, to make sure no residual proteins were in the washing buffers, we performed an SDS-PAGE of the supernatant related to the third washing step of the BC formation protocol, and we confirmed that no protein bands were detected (Fig. S3).

As highlighted in Fig. 2 and Fig. S2, the BCs formed on the six different NPs exhibited distinct protein band profiles when

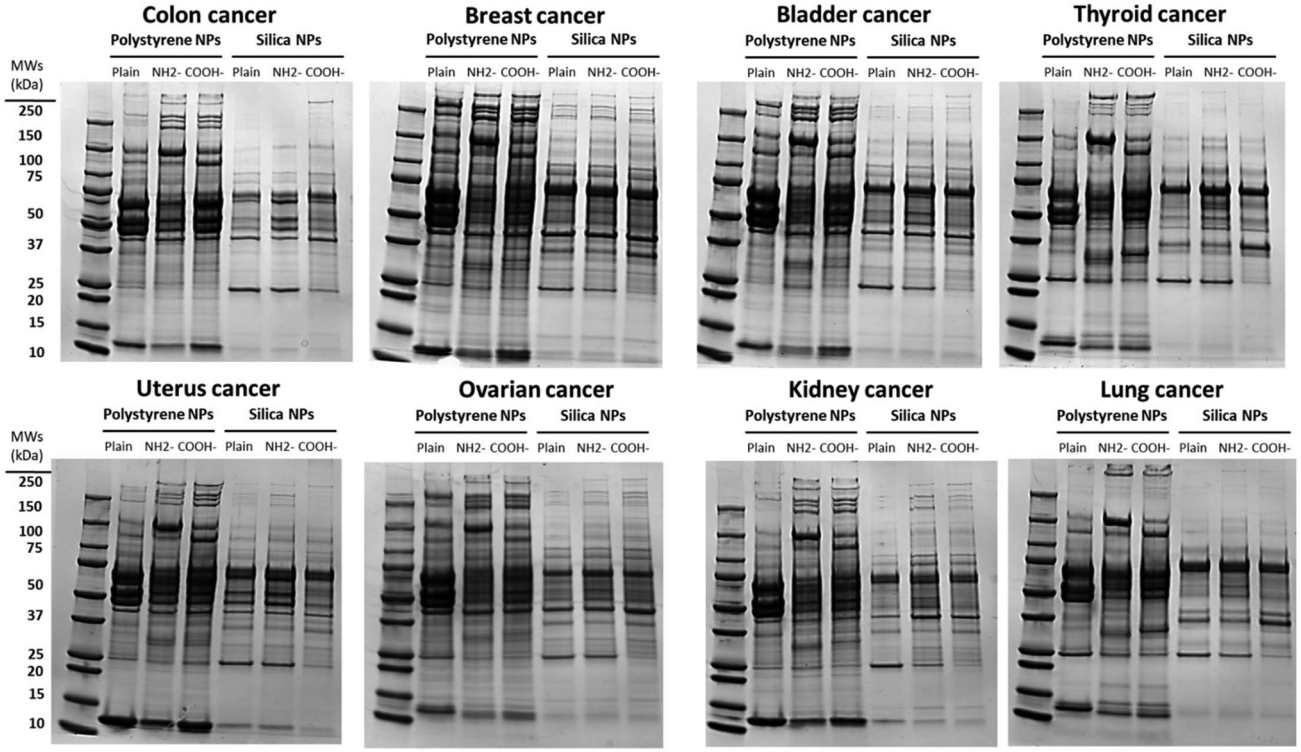

Fig. 2 BC profiles of polystyrene and silica NPs by SDS-PAGE analysis. Representative gels (one of five per cancer type) comparing the personalized corona of plain, amine- and carboxyl-modified NPs in human cancer plasma. Prominent bands observed around 66 kDa corresponding to serum albumin were consistently present, with variations in intensity depending on the NP type and plasma condition.

Table 2 Protein concentration within the BC as determined by Bradford assay. Results represent the mean ± SD of 5 independent cancer batches (n = 5) and 3 independent healthy batches (n = 3)

NPs	Kidney μg μL^{-1}	Ovarian μg μL^{-1}	Lung μg μL^{-1}	Thyroid μg μL^{-1}	Breast μg μL^{-1}	Bladder μg μL^{-1}	Uterus μg μL^{-1}	Colon μg μL^{-1}	Healthy μg μL^{-1}
Poly	1.62 ± 0.00	1.22 ± 0.03	0.72 ± 0.01	1.90 ± 0.10	1.53 ± 0.37	1.59 ± 0.63	0.95 ± 0.21	1.56 ± 0.15	1.03 ± 0.15
Poly-NH_2	0.88 ± 0.02	1.43 ± 0.02	0.80 ± 0.12	0.96 ± 0.03	0.85 ± 0.31	1.67 ± 0.22	1.00 ± 0.09	0.66 ± 0.15	2.10 ± 0.25
Poly-COOH	0.79 ± 0.02	2.41 ± 0.04	1.38 ± 0.16	1.40 ± 0.25	1.18 ± 0.68	0.80 ± 0.08	0.99 ± 0.00	1.03 ± 0.22	1.55 ± 0.41
Si	0.69 ± 0.04	1.30 ± 0.00	0.74 ± 0.11	0.51 ± 0.01	1.44 ± 0.10	0.98 ± 0.07	0.91 ± 0.09	0.83 ± 0.00	1.04 ± 0.25
Si-NH_2	1.22 ± 0.01	1.58 ± 0.08	0.89 ± 0.02	1.14 ± 0.22	1.61 ± 0.03	1.04 ± 0.14	1.24 ± 0.11	1.03 ± 0.01	2.15 ± 0.09
Si-COOH	0.86 ± 0.07	1.79 ± 0.01	0.82 ± 0.08	0.63 ± 0.05	1.50 ± 0.01	1.07 ± 0.06	0.83 ± 0.01	0.82 ± 0.06	1.85 ± 0.16

incubated in cancer plasmas. Indeed, a first-pass visual inspection reveals that the protein bands in the 10–15 kDa and 100–250 kDa molecular weight ranges derived from polystyrene NPs (Poly, Poly-NH_2, and Poly-COOH) were consistently more intense than those from the silica NPs (Si, Si-NH_2, and Si-COOH). This phenomenon can be primarily attributed to the distinct physicochemical properties of NPs, which play a critical role in shaping the pattern of adsorbed biomolecules and, consequently, influence the overall composition of the BC.[2,7,17] Specifically, polystyrene NPs exhibit a hydrophobic character, whereas silica NPs are characterized by hydrophilic surfaces.[42] In general, hydrophilic NP surfaces tend to reduce protein adsorption, while hydrophobic NPs preferentially bind proteins through interactions with their hydrophobic domains.[17,43,44]

To investigate the differential behavior of BCs formed on various NPs types incubated with healthy (n = 3) *vs.* cancer (n = 40) plasma, we analyzed the overall densitometric profiles obtained from one-dimensional SDS-PAGE gels, covering the full range of protein molecular weight (Fig. 3). Specifically, five patients for each of the eight cancer conditions were employed to collect plasma samples. All the relative gels obtained and analyzed are reported in Fig. S4. For BCs formed on polystyrene NPs (Poly, Poly-NH_2, and Poly-COOH), the protein profiles derived from cancer samples did not show significant differences compared to those from healthy plasma (Fig. 3a). In contrast, BCs generated on silica-based NPs exhibited clear distinctions between healthy and cancer-derived samples. Specifically, the total protein band intensities for Si, Si-NH_2, and Si-COOH NPs were significantly higher in cancer samples

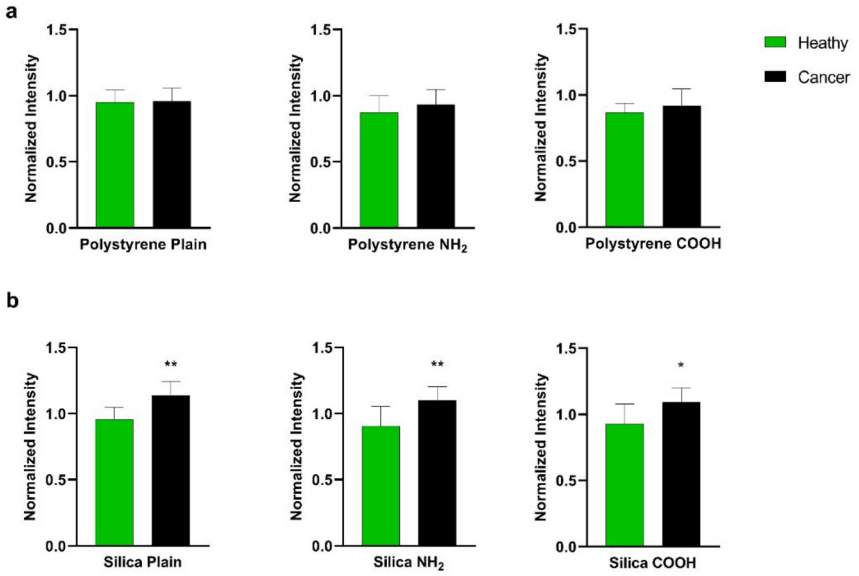

Fig. 3 Densitometric analysis of BCs of NPs in human cancer *vs.* healthy plasma. Densitometric analysis was performed using ImageJ to quantify the band intensity of 1D SDS-PAGE gels after incubation of polystyrene NPs (a) and silica NPs (b) with human plasma from cancer patients and healthy subjects. The *y*-axis represents band intensity normalized against the ladder. The total intensity of each gel lane was considered and averaged (cancer patients $n = 40$ *vs.* healthy controls $n = 3$). Unpaired *t*-tests determined statistical significance between groups. $*p \leq 0.05$, $**p \leq 0.01$.

compared to healthy controls (Fig. 3b). The performance of this diagnostic approach was evaluated through ROC curves and the corresponding AUC values. Results corroborate the results on proteins densitometric profile analysis, showing that the silica-based NPs as a good diagnostic potential. Indeed, AUC for Si, Si-NH_2, and Si-COOH were 0.93, 0.85, and 0.82 respectively (Fig. 4) while, polystyrene-based NPs AUC showed a poor ability to distinguish BCs of cancer patients from healthy subjects (AUC Poly = 0.55, AUC Poly-NH_2 = 0.68, and AUC Poly-COOH = 0.64) (Fig. S5). These findings suggest that BC analysis, particularly through total protein semi-quantification densitometric profiling, may serve as a valuable strategy for differentiating malignant from non-malignant states.

To assess the specificity of our method in discriminating not only healthy *versus* cancer plasma but also among different tumor types, we performed one-way ANOVA on entire lanes across different cancer conditions, comparing the same NP classes (Table S3). Results showed that the BC profile of Poly-COOH NPs for kidney cancer differed significantly from those of uterus (Tables S3b and f), bladder (S3c and f), colon (S3d and f), and breast (S3h and f) cancers. A similar pattern was observed for BC-coated Si NPs, which showed significant differences between kidney and uterus or breast cancers (Tables S3b, f and h). Additionally, the BC profile of Si-COOH NPs from kidney cancer was significantly different from that of uterus cancer plasma.

These results suggest that kidney cancer induces specific modifications in the BC composition of certain NPs, potentially reflecting a unique pathophysiological environment. Overall, our findings support the concept that disease-specific BC signatures can contribute to molecular discrimination among cancer types and may represent a step toward selective BC-based diagnostic tools.

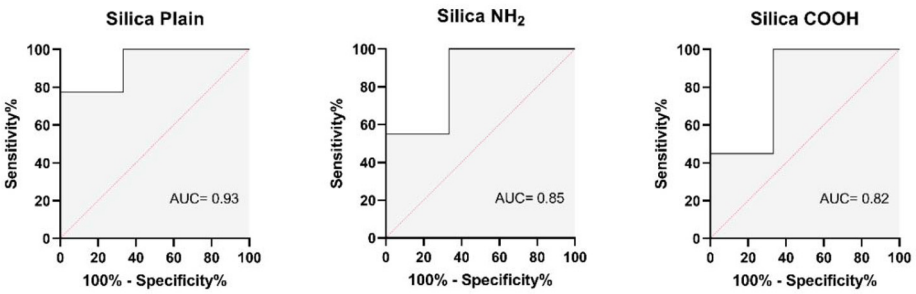

Fig. 4 ROC curves and AUC analyses of silica-based NPs densitometric data to validate the performance of the diagnostic test. AUC observed by the analysis of the cancers and healthy proteins derived from the BCs formed on the surface of Si (AUC = 0.93), Si-NH_2 (AUC = 0.85), and Si-COOH (AUC = 0.82).

Densitometric analysis of biomolecular corona profiles

To further assess the ability of BCs to distinguish between pathological and healthy conditions based on densitometric patterns, we compared the coronas formed on all six NP types following incubation with plasma from eight different cancer types (breast, ovarian, kidney, lung, colon, bladder, uterus, and thyroid) *vs.* healthy controls. The comparison was initially conducted by analyzing the global protein profiles within the 10–250 kDa molecular weight range (Fig. 5). To improve the resolution and interpretability of the SDS-PAGE analysis, we conducted a more detailed evaluation by segmenting the protein profiles into defined molecular weight intervals: <25 kDa (Fig. 6a and b), 25–75 kDa (Fig. 6c and d), and >75 kDa (Fig. S4). This stratified approach enabled us to better capture subtle, yet potentially informative, variations in protein abundance and migration between healthy and cancer-derived samples. In general, low molecular weight proteins

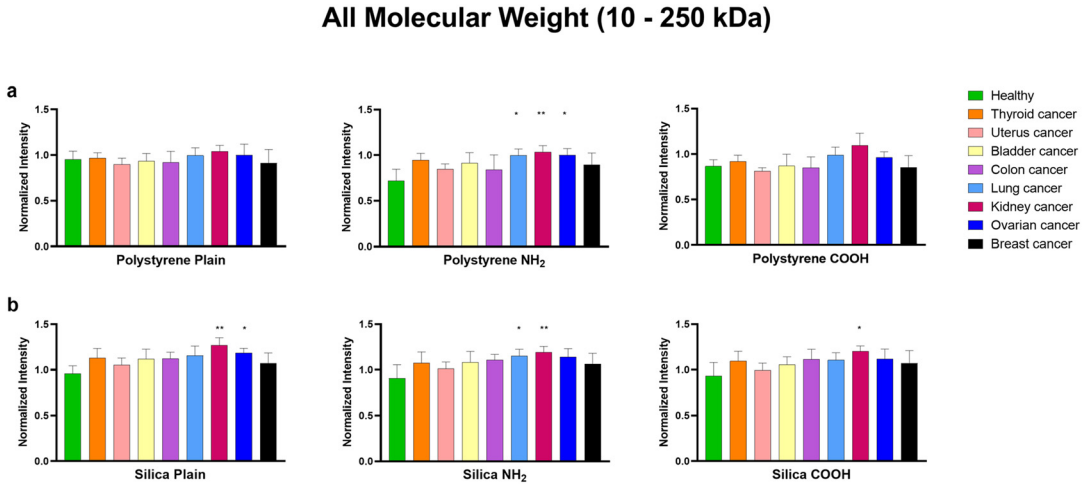

Fig. 5 Densitometric analysis of BCs of NPs in 8 human cancers *vs.* healthy plasma (10–250 kDa). BCs were formed on polystyrene NPs (a) and silica NPs (b) by incubation with human plasma from cancer patients (n = 40) and healthy controls (n = 3), and profiled by 1D SDS-PAGE. The total protein intensity of each gel lane was quantified using ImageJ. For comparative analysis, these values were normalized: the total intensity of the molecular weight ladder on each gel was assigned a reference value of one, and each sample lane's total intensity was expressed relative to this reference. The y-axis depicts the averaged normalized intensities. The statistical analysis was performed by one-way ANOVA with Tukey's test, each cancer *vs.* healthy control. *p value $\leq$ 0.05; **p value $\leq$ 0.01.

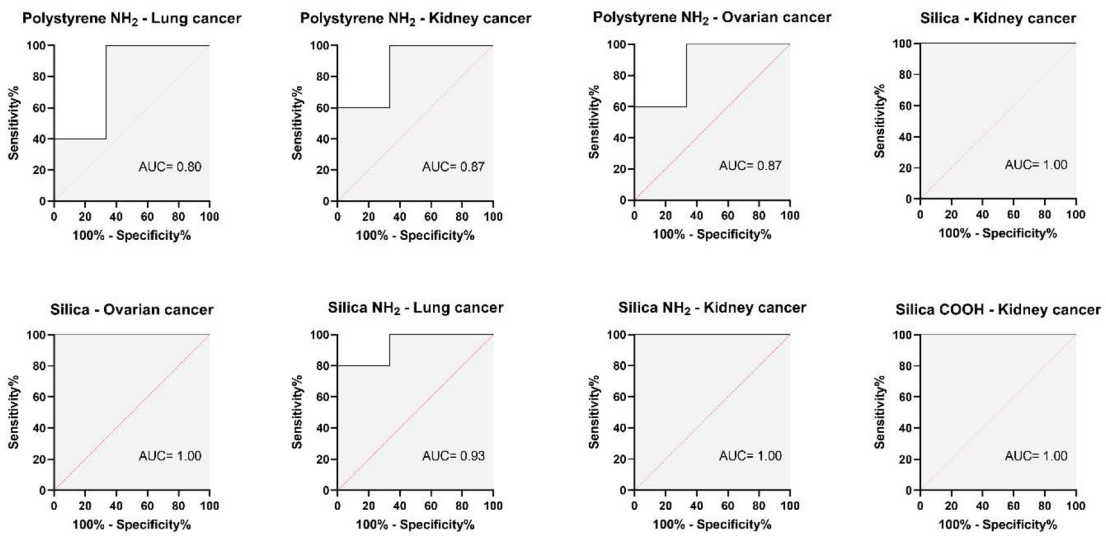

Fig. 6 ROC curves and AUC analyses of polystyrene and silica NPs densitometric data (10–250 kDa) to validate the performance of the diagnostic test. AUC observed by the analysis of the cancers and healthy proteins derived from the BCs formed on the surface of Poly-NH_2 lung cancer (AUC = 0.80), Poly-NH_2 kidney cancer (AUC = 0.87), Poly-NH_2 ovarian cancer (AUC = 0.87), Si kidney cancer (AUC = 1.00), Si ovarian cancer (AUC = 1.00), Si-NH_2 lung cancer (AUC = 0.93), Si-NH_2 kidney cancer (AUC = 1.00), and Si-COOH (AUC = 1.00).

(<25 kDa) are signaling polypeptides, cytokines, and other regulatory molecules that play key roles in cancer pathophysiology by exhibiting different adsorption patterns in tumor-associated BC.[45–48] Proteins with lower molecular weight, owing to reduced steric hindrance, exhibit a higher propensity to adsorb onto the NP surface *via* hydrophobic or electrostatic interactions. In line with this, the most pronounced statistical differences between healthy and cancer-derived samples were detected in the <25 kDa molecular weight range. The intermediate range (25–75 kDa) includes a wide array of high abundant plasma proteins, including albumin, several enzymes, transport proteins, and immunoglobulin fragments. This range is particularly informative for evaluating tumor-specific biomarkers in BCs composition, since different proteins implicated in cancer biology fall within this interval.[49–53] For instance, the heavy chains of immunoglobulin A and G (~37 kDa) are associated with the production of autoantibodies in tumorigenic patients as part of the immune response. In our study, silica NPs consistently outperformed polystyrene NPs in detecting proteins in this range, particularly in thyroid and lung cancer (Fig. 2, Fig. S4). Notably, in lung cancer plasmas, the 37 kDa band was consistently more intense in the biocorona adsorbed onto Silica-COOH NPs. This correlation may support the use of our approach as a preliminary cancer screening tool, providing information that can subsequently be validated by more advanced analyses such as mass spectrometry. High molecular weight proteins (>75 kDa), such as full-length immunoglobulins and large structural or adhesive proteins, might reflect systemic variation in proteins' expression or post-translational modifications associated with tumorigenesis.[54–56] In this molecular weight range, Immunoglobulin G (~ 150 kDa in non-reduced form) and complement C3 (185 kDa in non-reduced form) are often found in BC samples. Immunoglobulin G can mediate both antitumor cytotoxicity and tumor promotion through immune complex formation, while C3 is involved in tumor-promoting inflammation.[57] Given that C3 indeed can bind covalently to proteins in the corona and undergo dynamic exchange, it would be expected to find differential high molecular weight bands for various cancer type.[58] Usually, high molecular weight proteins are adsorbed on the NPs surface *via* multivalent binding or through complex conformational changes induced by the NPs environment.

Interestingly, the analysis of the BC in the entire 10–250 kDa protein range revealed that the Si-COOH NPs, and not the Poly-COOH, exhibited BC protein densitometric intensity profiles statistically significantly different between healthy plasma and kidney cancer plasma (Fig. 5). Notably, the BC of NH_2-functionalized NPs, both polystyrene and silica (Poly-NH_2 and Si-NH_2), discriminates kidney and lung, *vs.* control, with the BC of Poly-NH_2 showing capability of discrimination against ovarian cancer, too. The BC of unfunctionalized NPs lead to no discrimination power for polystyrene NPs, and the capability of discrimination of kidney and ovarian cancer *vs.* controls for silica NPs. Taken together, these results highlight that in the case of polystyrene NPs (Fig. 5a), the surface functionalization, particularly the amination, improved the discrimination power between cancer and healthy individuals. This does not apply to silica NPs for which the unfunctionalized NPs *per se* were able to discriminate two groups of cancer *vs.* control (Fig. 5b). Finally, Poly-NH_2 demonstrated the best performance in discriminating between cancerous and healthy samples for three over eight types of cancer (Fig. 5a).

To further explore the diagnostic potential of these NPs, we performed ROC curve analyses and calculated the related AUC for each NP in the protein range of 10–250 kDa (Fig. 6). Specifically, we obtained that Poly-NH_2 NPs showed good cancer discrimination performance with AUCs of 0.80 for lung cancer, 0.87 for kidney cancer, and 0.87 for ovarian cancer. Silica-based NPs confirmed their remarkable performance, with Si NPs achieving an AUC of 1.00 for both kidney and ovarian cancer, and Si-NH_2 NPs yielding AUCs of 0.93 for lung cancer and 1.00 for kidney cancer. Notably, Si-COOH NPs also reached an AUC of 1.00 for kidney cancer (Fig. 6). These findings further support the potential of the BCs profiles of NPs in effectively discriminating between cancer and healthy samples.

Densitometric analysis of the low molecular weight (<25 kDa) region of the BC proteins revealed that the modified NPs, both aminated and carboxylated, showed similar diagnostic capability, due to a BC's protein signature statistically significant different for kidney and ovarian cancers when compared to healthy plasma (Fig. 7), with that of Poly-NH_2 also able in discriminating the thyroid group. Finally, the BC profile on plain NPs showed a distinct signature for ovarian cancer, in the case of polystyrene (Fig. 7a), and for ovarian and kidney in the case of silica (Fig. 7b). This result on the silica NPs' BC overlaps what revealed in the analysis of the 10–250 kDa molecular weight range where unmodified silica NPs were able to differentiate two cancer types. An overlap is also present in the number of cancers discriminated with the Poly-NH_2 NPs in the two molecular weight ranges: interestingly, although a third cancer type was also identified in previous analyses, it was lung cancer rather than thyroid. In the 25–75 kDa molecular weight range, the BC profiles of both Poly-NH_2 and Poly-COOH NPs did not show statistically significant differences across the analyzed samples (Fig. 7c). Similar results are obtained on the Si-COOH NPs. In contrast, the BC associated with Si-NH_2 NPs exhibited statistically significant differences for lung, kidney, ovarian, and colon cancers (Fig. 7d). These findings for Si-NH_2 are consistent with results obtained from analyses in the 10–250 kDa and <25 kDa molecular weight ranges, where Si-NH_2 NPs were able to differentiate lung, kidney, and ovarian cancers. Interestingly, within this specific molecular weight range, a fourth cancer type, colon cancer, was identified. Finally, unmodified silica NPs showed significant discrimination for kidney and ovarian cancers (Fig. 7d), while unmodified polystyrene NPs were able to distinguish breast cancer (Fig. 7c). Analysis of BC proteins in the molecular weight range above 75 kDa revealed no statistically significant differences of cancer BC compared to healthy controls (Fig. S6).

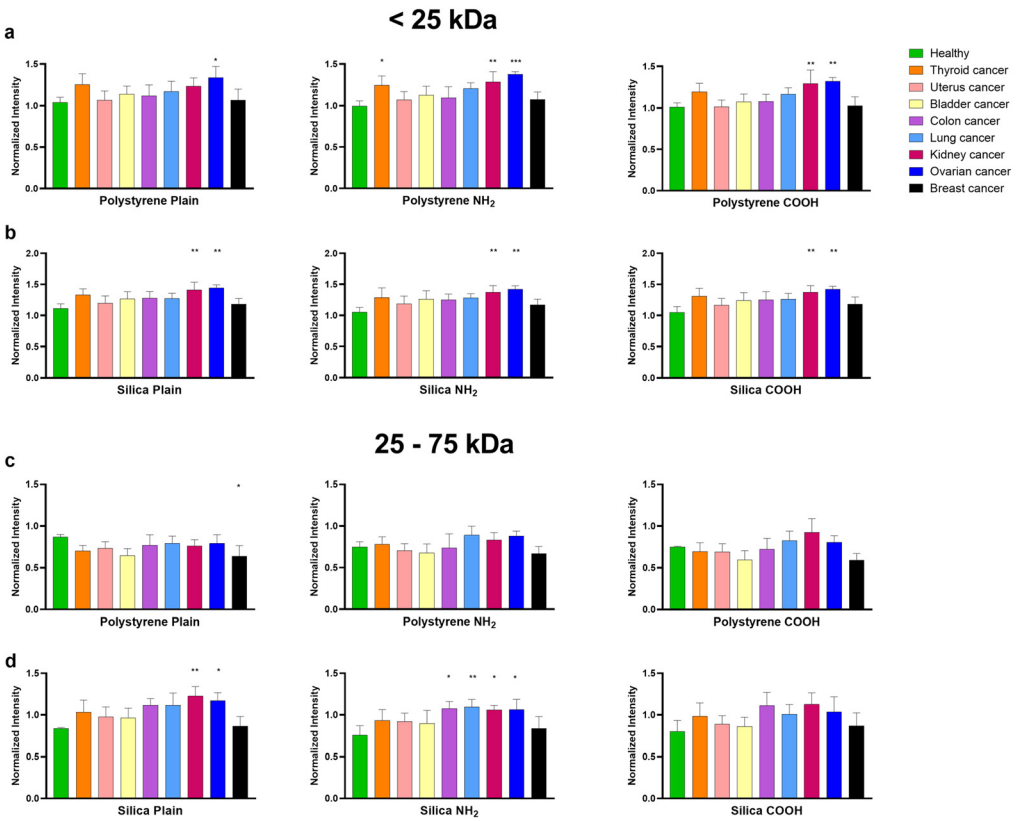

Fig. 7 Densitometric analysis of BCs of NPs in 8 human cancers *vs.* healthy plasma (≤ 25 kDa and 25–75 kDa). Densitometric analysis was performed using ImageJ to quantify the band intensity of 1D SDS-PAGE gels after incubation of the six NPs with human plasma from each type of cancer patients and healthy subjects. The *y*-axis represents band intensity normalized against the ladder. The intensity of protein bands into the gel at the molecular weight minor than 25 kDa (a and b) and included into the range of 25–75 kDa (c and d) were considered and averaged (cancer patients n = 5 for each cancer *vs.* healthy controls n = 3) for the densitometric analysis. The statistical analysis was performed by one-way ANOVA with Tukey's test, each cancer *vs.* healthy control. *p value ≤ 0.05; **p value ≤ 0.01; ***p value ≤ 0.001.

Conclusions

Much evidence of the last decade suggests that the BC can enrich specific biomolecules and/or reveal distinct biomolecular patterns within biological fluids, enabling the exploitation of the BC for diagnostic purposes. Here, we hypothesized that a dataset of BC protein signatures can be generated by utilizing a panel of NPs with diverse physicochemical properties (polystyrene and silica, with plain, amino-, and carboxyl-functionalization). These signatures, even when analyzed by a relatively cost-friendly and straightforward SDS-PAGE followed by semi-quantitative analysis, showed an ability to discriminate between healthy individuals and patients with cancer. The selected cancers (*e.g.*, breast, ovarian, kidney, lung, colon, bladder, uterine, and thyroid) represent common and clinically significant solid tumors that vary in tissue origin and biological behavior. Studying these diverse types allows evaluation of whether the BC can capture tumor-specific signatures across a broad spectrum of cancer types.

Notably, we found that the most effective discrimination between healthy plasma and cancer plasma was achieved when analyzing proteins in the lower (<25 kDa) and intermediate (25–75 kDa) molecular weights ranges. In general, the amination was the surface functionalization that better enabled the formation of distinct BC profiles allowing for the discrimination of up to four cancer types from healthy controls. Two types of cancer were discriminated more frequently, and those are ovarian and kidney. Among the NPs employed, the silica NPs in general have demonstrated to perform better. The observed differences between polystyrene and silica NPs likely arise from their distinct physicochemical properties, such as surface chemistry, hydrophilicity, and charge. Silica NPs are more hydrophilic and possess surface silanol groups, which may favor the selective adsorption of certain plasma proteins that are more reflective of disease states. This difference in surface protein interactions could enhance their capability to capture subtle variations in the plasma proteome associated with cancer, resulting in a more distinct and informative BC pattern. In contrast, polystyrene NPs, being more hydrophobic, may form coronas dominated by high-abundance plasma proteins, which could mask cancer-specific signatures. While this hypothesis aligns with literature on BC formation, we acknowledge that a deeper mechanistic investi-

gation is necessary. Future work will aim to systematically compare the BC profiles on different nanomaterials and correlate them with NP surface properties and diagnostic performance. In this context, it will also be important to explore the role of positively charged NPs. Although excluded from the present study due to their tendency to adsorb abundant plasma proteins non-specifically, cationic NPs can nevertheless capture proteins with atypical charge distributions or that interact *via* non-electrostatic mechanisms. Their inclusion could therefore expand the diversity of detectable BC patterns, offering complementary diagnostic insights. Despite on a limited number of plasmas, our findings are relevant to the field of cancer nanotechnology and suggest that this method of analysis could allow minimally invasive diagnosis of cancer through a specific cancer-associated BC signature. Such approach could represent a cheaper alternative to the mass spectrometry-based methods for BC patterns identification. With larger sample sizes on selected cancer types in the future, we aim to reinforce this data by validating the diagnostic performance also on an independent validation test to further use this approach in the identification of potential BC 'fingerprints' to be associated with specific diseases. Additionally, machine learning can be used to develop more robust and sophisticated classification tools.

Author contributions

Antonietta Greco: data curation, formal analysis, investigation, methodology, and writing. Esther Imperlini: data curation, formal analysis, and methodology. Gha Young Lee: investigation, methodology, and writing. Maciej Serda: investigation, methodology. Santiago Alonso Tobar Leitão: investigation, methodology. Claudia Corbo: conceptualization, formal analysis, investigation, funding acquisition, methodology, project administration, supervision, and writing.

Conflicts of interest

There are no conflicts to declare.

Data availability

The data supporting this article have been included as part of the supplementary information (SI). Supplementary information is available. See DOI: https://doi.org/10.1039/d5nr03082j.

Acknowledgements

This work is dedicated by C.C. to her late father, whose memory continues to inspire her. He taught her the value of perseverance and the importance of always believing in her work and aspirations. This work was supported by the Italian Ministry of University and Research (MUR), Call PRIN 2022 (2022WN89PC), Italian Ministry of Health RC 2022 (L2089), and University of Milan Bicocca (FAQC 2022) to C.C. C.C. discloses that she receives royalties for her licensed patent. Open access publishing facilitated by Universita degli Studi di Milano-Bicocca, as part of the Wiley - CRUI-CARE agreemen.

References

1 V. Kopatz, K. Wen, T. Kovács, A. S. Keimowitz, V. Pichler, J. Widder, A. D. Vethaak, O. Hollóczki and L. Kenner, *Nanomaterials*, 2023, **13**, 1404.
2 A. Greco and C. Corbo, *Nanomedicine*, 2025, **20**(11), 1219–1222.
3 A. Salvati, *Curr. Opin. Biotechnol*, 2024, **87**, 103101.
4 C. Corbo, R. Molinaro, A. Parodi, N. E. Toledano Furman, F. Salvatore and E. Tasciotti, *Nanomedicine*, 2016, **11**, 81–100.
5 R. Liam-Or, F. N. Faruqu, A. Walters, S. Han, L. Xu, J. T. W. Wang, J. Oberlaender, A. Sanchez-Fueyo, G. Lombardi, F. Dazzi, V. Mailaender and K. T. Al-Jamal, *Nat. Nanotechnol.*, 2024, **19**(6), 846–855.
6 Y. Zhang, W. Xiao, S. He, X. Xia, W. Yang, Z. Yang, H. Hu, Y. Wang, X. Wang, H. Li, Y. Huang and H. Gao, *J. Controlled Release*, 2024, **368**, 42–51.
7 A. Greco and C. Corbo, *Small Sci.*, 2025, **5**(9), 2500206.
8 S. P. Carneiro, A. Greco, E. Chiesa, I. Genta and O. M. Merkel, *Expert Opin. Drug Delivery*, 2023, **20**, 471–487.
9 S. A. Dilliard, Y. Sun, M. O. Brown, Y. C. Sung, S. Chatterjee, L. Farbiak, A. Vaidya, X. Lian, X. Wang, A. Lemoff and D. J. Siegwart, *J. Controlled Release*, 2023, **361**, 361–372.
10 S. A. Dilliard, Q. Cheng and D. J. Siegwart, *Proc. Natl. Acad. Sci. U. S. A.*, 2021, **118**(52), e2109256118.
11 M. Qiu, Y. Tang, J. Chen, R. Muriph, Z. Ye, C. Huang, J. Evans, E. P. Henske and Q. Xu, *Proc. Natl. Acad. Sci. U. S. A.*, 2022, **119**(8), e2116271119.
12 F. Giulimondi, E. Vulpis, L. Digiacomo, M. V. Giuli, A. Mancusi, A. L. Capriotti, A. Laganà, A. Cerrato, R. Zenezini Chiozzi, C. Nicoletti, H. Amenitsch, F. Cardarelli, L. Masuelli, R. Bei, I. Screpanti, D. Pozzi, A. Zingoni, S. Checquolo and G. Caracciolo, *ACS Nano*, 2022, **16**, 2088–2100.
13 Z. Luo, L. Lu, W. Xu, N. Meng, S. Wu, J. Zhou, Q. Xu, C. Xie, Y. Liu and W. Lu, *J. Controlled Release*, 2022, **346**, 32–42.
14 Y. Peng, Y. Cong, Y. Lei, F. Sun, M. Xu, J. Zhang, L. Fang, H. Hong and T. Cai, *Adv. Healthc. Mater.*, 2022, **11**(8), 2102270.
15 N. Kamaly, O. C. Farokhzad and C. Corbo, *Nanoscale*, 2022, **14**, 1606–1620.
16 E. Imperlini, L. Di Marzio, A. Cevenini, M. Costanzo, N. d'Avanzo, M. Fresta, S. Orru, C. Celia and F. Salvatore, *Nanoscale Adv.*, 2024, **6**, 4434–4449.
17 S. Wang, J. Zhang, H. Zhou, Y. C. Lu, X. Jin, L. Luo and J. You, *J. Controlled Release*, 2023, **360**, 15–43.

18 C. Corbo, A. A. Li, H. Poustchi, G. Y. Lee, S. Stacks, R. Molinaro, P. Ma, T. Platt, S. Behzadi, R. Langer, V. Farias and O. C. Farokhzad, *Adv. Healthc. Mater.*, 2021, **10**(2), 2000948.
19 M. Hadjidemetriou, J. Rivers-Auty, L. Papafilippou, J. Eales, K. A. B. Kellett, N. M. Hooper, C. B. Lawrence and K. Kostarelos, *ACS Nano*, 2021, **15**(4), 7357–7369.
20 L. Papafilippou, A. Claxton, P. Dark, K. Kostarelos and M. Hadjidemetriou, *Nanoscale*, 2020, **12**, 10240–10253.
21 G. Y. Lee, A. A. Li, I. Moon, D. Katritsis, Y. Pantos, F. Stingo, D. Fabbrico, R. Molinaro, F. Taraballi, W. Tao and C. Corbo, *Small*, 2024, **20**(10), 2306168.
22 S. A. Tobar Leitão, G. Sausen, Y. Liu, Y. Yu, A. Greco, R. Molinaro, O. C. Farokhzad, C. Corbo and P. Libby, *Small*, 2025, 2503915.
23 M. D. P. Chantada-Vázquez, A. C. López, M. García-Vence, B. Acea-Nebril, S. B. Bravo and C. Núñez, *Int. J. Mol. Sci.*, 2020, **21**, 1–18.
24 L. Digiacomo, K. Jafari-Khouzani, S. Palchetti, D. Pozzi, A. L. Capriotti, A. Laganà, R. Zenezini Chiozzi, D. Caputo, C. Cascone, R. Coppola, G. Flammia, V. Altomare, A. Grasso, M. Mahmoudi and G. Caracciolo, *Nanoscale*, 2020, **12**, 16697–16704.
25 J. E. Blume, W. C. Manning, G. Troiano, D. Hornburg, M. Figa, L. Hesterberg, T. L. Platt, X. Zhao, R. A. Cuaresma, P. A. Everley, M. Ko, H. Liou, M. Mahoney, S. Ferdosi, E. M. Elgierari, C. Stolarczyk, B. Tangeysh, H. Xia, R. Benz, A. Siddiqui, S. A. Carr, P. Ma, R. Langer, V. Farias and O. C. Farokhzad, *Nat. Commun.*, 2020, **11**(1), 3662.
26 R. Di Santo, L. Digiacomo, E. Quagliarini, A. L. Capriotti, A. Laganà, R. Z. Chiozzi, D. Caputo, C. Cascone, R. Coppola, D. Pozzi and G. Caracciolo, *Front. Bioeng. Biotechnol.*, 2020, **8**, 536082.
27 D. Caputo, A. Coppola, E. Quagliarini, R. Di Santo, A. L. Capriotti, R. Cammarata, A. Laganà, M. Papi, L. Digiacomo, R. Coppola, D. Pozzi and G. Caracciolo, *Cancers*, 2022, **14**, 19–4658.
28 V. Colapicchioni, M. Tilio, L. Digiacomo, V. Gambini, S. Palchetti, C. Marchini, D. Pozzi, S. Occhipinti, A. Amici and G. Caracciolo, *Int. J. Biochem. Cell Biol.*, 2016, **75**, 180–187.
29 R. Di Santo, E. Quagliarini, L. Digiacomo, D. Pozzi, A. Di Carlo, D. Caputo, A. Cerrato, C. M. Montone, M. Mahmoudi and G. Caracciolo, *Biomater. Sci.*, 2021, **9**, 4671–4678.
30 D. Caputo, M. Papi, R. Coppola, S. Palchetti, L. Digiacomo, G. Caracciolo and D. Pozzi, *Nanoscale*, 2016, **9**, 349–354.
31 L. Digiacomo, E. Quagliarini, D. Pozzi, R. Coppola, G. Caracciolo and D. Caputo, *Cancers*, 2023, **15**, 2983.
32 L. Digiacomo, D. Caputo, R. Cammarata, V. La Vaccara, R. Coppola, E. Quagliarini, M. Iacobini, S. Renzi, F. Giulimondi, D. Pozzi, G. Caracciolo and H. Amenitsch, *Nanoscale*, 2025, **17**, 7066–7075.
33 S. Sheibani, K. Basu, A. Farnudi, A. Ashkarran, M. Ichikawa, J. F. Presley, K. Huy Bui, M. Reza Ejtehadi, H. Vali and M. Mahmoudi, *Nat. Commun.*, 2021, **12**(1), 573.
34 W. Wu, Q. Wu, Q. Liu, Y. Li, P. Ren, Y. Wu and F. Chen, *Chin. J. Anal. Chem.*, 2023, **51**, 100246.
35 M. Dell'Aglio, Z. Salajková, A. Mallardi, M. C. Sportelli, J. Kaiser, N. Cioffi and A. De Giacomo, *Talanta*, 2021, **235**, 122741.
36 H. Lee and P. H. Lee, *Small*, 2020, **16**, 1906598.
37 G. Bashiri, M. S. Padilla, K. L. Swingle, S. J. Shepherd, M. J. Mitchell and K. Wang, *Lab Chip*, 2023, **23**, 1432.
38 M. P. Vincent, S. Bobbala, N. B. Karabin, M. Frey, Y. Liu, J. O. Navidzadeh, T. Stack and E. A. Scott, *Nat. Commun.*, 2021, **12**, 1–18.
39 D. Prozeller, C. Rosenauer, S. Morsbach and K. Landfester, *Biointerphases*, 2020, **15**, 3.
40 S. Palchetti, V. Colapicchioni, L. Digiacomo, G. Caracciolo, D. Pozzi, A. L. Capriotti, G. La Barbera and A. Laganà, *Biochim. Biophys. Acta*, 2016, **1858**, 189–196.
41 M. Kokkinopoulou, J. Simon, K. Landfester, V. Mailänder and I. Lieberwirth, *Nanoscale*, 2017, **9**, 8858–8870.
42 B. Véliz, A. Orpella, M. Dominguez and S. Bermejo, *Mater. Chem. Phys.*, 2020, **243**, 122620.
43 K. Wang, C. Zhou, Y. Hong and X. Zhang, *Interface Focus*, 2012, **2**, 259–277.
44 V. Francia, D. Montizaan and A. Salvati, *Beilstein J. Nanotechnol.*, 2020, **11**, 338–353.
45 A. V. S. Faria, E. M. B. Fonseca, H. G. Cordeiro, S. P. Clerici and C. V. Ferreira-Halder, *Cell. Mol. Life Sci.*, 2021, **78**, 1263–1273.
46 H. Owji, N. Nezafat, M. Negahdaripour, A. Hajiebrahimi and Y. Ghasemi, *Eur. J. Cell Biol.*, 2018, **97**, 422–441.
47 S. Vimalraj, *Int. J. Biol. Macromol.*, 2022, **221**, 1428–1438.
48 C. T. Kureshi and S. K. Dougan, *Cancer Cell*, 2024, **43**, 15.
49 J. Wu, Z. Yang, J. Ding, S. Hao, H. Chen, K. Jin, C. Zhang and X. Zheng, *Hum. Genomics*, 2025, **19**, 17.
50 P. J. van der Watt, M. O. Okpara, A. Wishart, M. I. Parker, N. C. Soares, J. M. Blackburn and V. D. Leaner, *Int. J. Cancer*, 2022, **150**, 347–361.
51 M. P. A. Davies, T. Sato, H. Ashoor, L. Hou, T. Liloglou, R. Yang and J. K. Field, *EBioMedicine*, 2023, **93**, DOI: 10.1016/j.ebiom.2023.104686.
52 P. Patel, Z. Jamal and K. Ramphul, *Encycl. Respir. Med.*, 2023, **1–4**, V2-314–V2-320.
53 L. O. Elingaard-Larsen, M. G. Rolver, E. E. Sørensen and S. F. Pedersen, *Rev. Physiol., Biochem. Pharmacol.*, 2022, **182**, 1–38.
54 M. Kędzierska and M. Bańkosz, *J. Clin. Med.*, 2024, **13**, 7131.
55 A. K. Saldaña-Villa and R. Lara-Lemus, *Int. J. Med. Sci.*, 2023, **20**, 1662–1670.
56 N. Ebrahimi, E. Fardi, H. Ghaderi, S. Palizdar, R. Khorram, R. Vafadar, M. Ghanaatian, F. Rezaei-Tazangi, P. Baziyar, A. Ahmadi, M. R. Hamblin and A. R. Aref, *Cell. Mol. Life Sci.*, 2023, **80**(4), 104.
57 D. Ain, T. Shaikh, S. Manimala and B. Ghebrehiwet, *Fac. Rev.*, 2021, **10**, 80.
58 F. Chen, G. Wang, J. I. Griffin, B. Brenneman, N. K. Banda, V. M. Holers, D. S. Backos, L. Wu, S. M. Moghimi and D. Simberg, *Nat. Nanotechnol.*, 2016, **12**, 387.